Stony Brook University

Preparation and sensing properties of FSP processed WO_3 nano sensor

A Thesis Presented

by

Jiahao Huang

to

The Graduate School

in Partial Fulfillment of the

Requirements

for the Degree of

Master of Science

in

Materials Science and Engineering

Stony Brook University

August 2014

Stony Brook University

The Graduate School

Jiahao Huang

We, the thesis committee for the above candidate for the

Master of Science degree, hereby recommend

acceptance of this thesis.

Pelagia Irene (Perena) Gouma
Professor Department of Materials Science and Engineering

Milutin Stanaćević
Associate Professor Department of Electrical and Computer Engineering

Sanford Simon
Professor Departments of Biochemistry and Cell Biology and Pathology

This thesis is accepted by the Graduate School

Charles Taber
Dean of the Graduate School

Abstract of the Thesis

Preparation and sensing properties of FSP processed WO_3 nano sensor

by

Jiahao Huang

Master of Science

in

Materials Science and Engineering

Stony Brook University

2014

Nano-scale tungsten trioxide (WO_3) particles have been synthesized by the flame spray pyrolysis method and a 3×3 mm^2 sensor was made by the drop-coating method using the nanoparticles as the active element. After heat-treatment at 500 °C, the materials structure and morphology were characterized by X-ray diffraction, transmission electron microscopy and Raman spectroscopy. Sensing tests were carried out at 200 and 350 °C respectively, down to a trace nitric oxide concentration of 100 parts per billion. The sensor sensitivity was remarkable at these two working conditions employed in this work, providing evidence for the importance of flame spray pyrolysis method as a scalable sensor materials processing technique.

Table of Contents

List of Figures

List of Table

Acknowledgements

I would like to express my appreciation and thanks to my advisor Professor Gouma, you have been a tremendous mentor to me. Your guidance and support throughout my master study is priceless. I would also like to thank my committee members, Professor Simon and Professor Milutin for serving as my committee members and all the advice you gave me. I would especially like to thank my lab mates Jusang Lee, Shantanu Sood, Gagan Jodhani and Wen Ling Liao. You have helped me a lot in my study and life.

Special thanks to my family. Words couldn't express how grateful I am to my parents for giving me all your supports in these years.

This thesis work has been supported by the SHB NSF grant IIS 1231761 and Brookhaven National Lab proposal 31878.

Chapter 1 Introduction

1.1 Biomarkers in human exhaled breath

Breathing is one of the most important metabolic processes of all living creatures, including human beings and it takes place in an atmosphere of nitrogen, oxygen, carbon dioxide and other gases [1]. Basically, the breathing process is made up of two steps: inhalation and exhalation [2]. The oxygen inhaled from the air is delivered to where it is needed in human body and carbon dioxide is removed from it to the air. Aside from the oxygen and carbon dioxide exchange, more gases are involved in this metabolic process. There are 30 compounds, out of 400 or more, in human exhaled breath that have been considered potential biomarkers of different types of diseases [3-5]. Among them, nitric oxide has been studied as a biomarker for oxidative stress and it's also related to cardiac disease and pulmonary disease [6]; carbon monoxide is a biomarker for cardiovascular disease, diabetes, nephritis, bilirubin production [7]. Ammonia is a biomarker of renal failure [7]; while isoprene relates to cholesterol levels in human blood [8].

1.1.1 Nitric Oxide (NO)

Nitric oxide, or nitrogen monoxide, is a molecule with chemical formula NO. NO from human body is produced from L-arginine by at least three isoforms of enzyme NO synthase (NOS) [9]. Two of these are activated by small rise in intracellular calcium concentration, including neuronal NOS and endothelial NOS which are expressed in neurons and endothelial cells respectively. However, other cells also express these two isoforms. The third enzyme is inducible NOS, which has a greater level of activity and is independent of calcium concentration. It may be induced by inflammatory cytokines and viral infections showing increased expression

in inflammatory diseases [10]. NO has been studied as biomarker for several airway diseases [11], especially asthma.

1.1.2 Isoprene

Isoprene (2-methylbutadiene-1, 3) is one of the major volatile organic compounds produced by human body and measuring the amount of isoprene in human exhaled air was expected to provide a non-invasive method for monitoring blood cholesterols level.

1.2 Breath analysis methods

Breath analysis is attracting more and more attention because of its noninvasiveness, and easy repeatability. Nowadays, there are different types of techniques to identify specific gas with ultra-low concentration down to parts per million (ppm) or even parts per billion (ppb) levels. Spectrometry and chemical sensing are two main categories.

1.2.1 Spectrometry technique

Among the most common spectrometry techniques in the market are:

i.) Gas chromatography-mass spectrometry (GC-MS) [12]: GC-MS is made up of two parts: gas chromatography (GC) portion separates the chemical mixture into pulses of pure chemicals, which is based on the analyte's volatility and the mass spectrometer (MS) identifies, and quantifies the chemicals, which is based on the analyte's chemical structure.

ii.) Proton transfer reaction mass spectrometry (PTR-MS) [13]: The working method of PTR-MS is the chemical ionization, by proton transfer, of a gas sample inside of a drift tube. The proton source is normally H_3O^+. The fixed length of the drift tube provides a fixed reaction time for the ions when they pass along the tube: the ion residence time and reaction time can be measured or calculated from ion transport properties. If the proton donor concentration is largely

unchanged by the addition of the analyte sample, then measurement of the (proton donor) / (protonated acceptor) ion signal ration allows the absolute concentration of the acceptor molecules to be calculated from a simple kinetic analysis. Consequently, by combining reaction kinetics with mass spectrometry, it is possible to both identify and quantify individual organic gases on a relatively short time scale with high sensitivity.

iii.) Selected ion flow tube mass spectrometry (SIFT-MS) [14]: SIFT-MS relies on chemical ionization of the trace gas molecules in air/breath samples introduced into helium carrier gas using H_3O^+, NO^+ and O_2^+ precursor ions. Reactions between the precursor ions and trace gas molecules proceed for an accurately defined time, the precursor and product ions being detected and counted by a downstream mass spectrometer, thus effecting quantification. Absolute concentrations of trace gases in single breath exhalation can be determined by SIFT-MS down to ppb levels, obviating sample collection and calibration.

iv.) Ion mobility spectrometry (IMS) [15]: IMS is used to separate and identify ionized molecules in gas phase based on their mobility in a carrier buffer gas. It provides a combination of detection features such as high sensitivity (ppb), fast response (a few seconds), small size (wearable), low power consumption (about 4 AA batteries) and low cost.

Other spectroscopy techniques include Fourier transform infrared spectroscopy (FTIR) [16], laser absorption spectroscopy (LAS) [17], etc.

There are several nitric oxide analyzers in the market: The Sievers Nitric Oxide Analyzer (NOA™) and the Aerocrine NIOX MINO®. Both of them measure nitric oxide by a chemiluminescent reaction with ozone [18]:

$$NO + O_3 \rightarrow NO_2^* + O_2$$

$$NO_2^* \rightarrow NO_2 + h\nu$$

Exhaled breath is injected into a chamber then nitric oxide in the breath reacts with ozone, yielding NO_2, O_2 and photons, which are captured by the photomultiplier tube that analyzes proportional value of nitric oxide in the breath.

These methods above are capable of providing good sensitivity and selectivity of target biomarkers in human exhaled breath. However, they have limitations such as: they are bulky, expensive and/or not capable of real-time detection.

1.2.2 Chemical sensing

A chemical sensor transforms chemical information, like composition, concentration, pH level, partial pressure, presence of one particular molecule, etc., into analytical signal.

The ideal chemical sensor is an inexpensive, portable, foolproof device that responds with perfect and instantaneous selectivity to a particular target chemical substance (analyte) present in any desired medium in order to produce a measurable signal output at any required analyte concentration [19].

Most of chemical sensors are made up of two basic components in series: a receptor and a transducer. In the most cases, the receptor interacts with analyte molecules then changes its properties, from which the transducer would get a secondary signal, mostly electrical signal. A thin layer in the surface of the chemical sensor which is able to interact with analyte molecules, catalyze a reaction or participate in a chemical equilibrium with the analyte. The most important one among the interaction process for chemical sensors are adsorption and ion exchange. Signal

processing by means of electrical instrumentation requires the sensors to include transducers to transform non-electric quantities into electric ones like voltage, current, resistance or conductance. An additional receptor layer may be needed for some sensors (e.g. biosensors) while receptor operation is an inherent function of the transducer for others.

Below is the classification of chemical sensors according to the operating principle of the transducer [20]:

- Optical sensors transform changes of optical phenomena, following absorbance, reflectance, luminescence, fluorescence, refractive index, optothermal effect and light scattering
- Electrochemical sensors transform the effect of the electrochemical interaction analyte-electrode into a useful signal; among them are voltammetric sensors, potentiometric sensors, chemically sensitized field effect transistor and potentiometric solid electrolyte gas sensors.
- Electrical sensors based on measurements of the signal that arises from the change of electrical properties caused by the interaction of the analyte where no electrochemical processes take place. These included metal oxide semiconductor sensors used principally as gas phase detectors which will be discussed later, based on reversible redox processes of analyte gas components, organic semiconductor sensors, electrolyte conductivity sensors and electric permittivity sensors.
- Mass sensitive sensors transform the mass change at a specially modified surface into a change of a property of the support material. These include piezoelectric sensors and surface acoustic wave sensors.
- Magnetic sensors based on the change of paramagnetic properties of a gas being analyzed.
- Thermometric sensors based on the measurement of the heat effects of a specific chemical reaction or absorption that involve the analyte.

- Other sensors, mainly based on emission or absorption on radiation.

1.3 Chemo-resistive gas sensors

Chemo-resistive gas sensor is a term used for gas sensing element based on measuring changes of its resistance in the presence of varying concentrations of the analyte gas. The first commonly used commercial chemo-resistive gas sensor is the so-called Taguchi sensor [21]. This type of sensor uses doped metal oxides with noble metal to react to reducing gas at a certain temperature. This sensor is inexpensive and has a long life, as long as 10 years in some cases.

The gas sensing mechanism for metal oxide semiconductor gas sensor is not completely clear yet; however there are possible pathways reported.

When the metal oxide semiconductor sensor is in air, oxygen absorbs on the surface and dissociates to form O^-, which extracts the electron from the semiconductor to the oxygen. This act of electron extraction tends to increase the resistance (assuming the semiconductor is an n-type one whose majority charge carries are electrons) of the sensor. In the presence of combustible gases, the absorbed O^- reacts with them and electrons are re-injected to the semiconductor that tends to decrease the resistance of it. A competition between oxygen removing the electrons and combustible gases re-injecting the electrons comes to a steady state which the resistance of the metal oxide is determined [22].

Another model that exists or co-exists is that the combustible gas would extract a lattice-oxygen from the metal oxide, leaving vacancies that act as donors. The oxygen from the air tends to re-oxidize the metal oxide and remove the donor vacancies. A competition between the combustible gas creating vacancies as donors and the oxygen removing the vacancies exists [23].

1.3.1 Parameters of chemo-resistive gas sensor

To evaluate the performance of a certain gas sensor or compare it to others, several parameters are listed here:

- Sensitivity: Sensitivity (S) can be defined as the magnitude of response of a sensor to a specific analyte gas. Usually there are two different ways to define sensitivity according to the application. Assume R_a as the resistance of sensor in the air and R_g as the resistance of sensor in the analyte gas. The first definition one is called relative sensitivity,

$$S = \frac{\Delta R}{R_a} = \frac{|R_g - R_a|}{R_a}$$

The other one is a normalized one, which is:

$$S = \frac{R_g}{R_a}$$

when $R_g > R_a$, or

$$S = \frac{R_a}{R_g}$$

when $R_g < R_a$.

- Selectivity: Selectivity is the ability of a sensor to distinguish one specific gas or a group of gases from other interfering gases and it's a very important factor for sensor selection.
- Stability: The ability of a sensor to reproduce the same response to the same input in a long period. It is a very important characteristic of sensor for practical use.
- Response time and recovery time: The ideal sensor responds to the target analyte gas immediately and recovers to its origin status right after the signal is withdrawn. However, in practice it takes some time for the resistance of the sensor to go to the final value or go back to the baseline. To determine these two values, we can take the length of time for the resistance to

go from R_a to $10\%R_g+90\%R_a$ as response time and the length of time for the resistance to go from R_a to $10\%R_a+90\%R_g$ as recovery time, respectively.

1.3.2 Grain size effect on chemical sensing

The influence of grain size (D) on the resistance and gas sensitivity was investigated thoroughly by Yamazoe et al. about twenty years ago [24]. The absorption of O_2 in air or NO_2 (or other oxidizing gases) on WO_3 induces an electron-depleted space-charge layer in the particles. When D is larger than twice the thickness (L) of the space-charge layer, the space charge layer occupies the surface of WO_3 particles so the electrical resistance of the device is determined by the electron transport across each grain boundary. In this case, the resistance is independent of D. When D decreases to be smaller than 2L, in another case, the entire grain of WO_3 is in the space-charge region so the resistance of the device is determined not only by the resistance of grain boundary but also by the bulk resistance of each grain. As the D decreases, the electron densities at the surface and bulk decrease. In this case, the smaller the grain size, the higher the resistance of the sensor. They found out that L is determined by Debye length (L_D) and eV_s (height of Schottky barrier) at the surface. Since L_D is intrinsic value for WO_3, eV_s value is the main factor of L, which depends on the sort and amount of absorbates formed on the WO_3 surface. The dependence of sensitivity on D could be explained in a similar way. When D is larger than 2L, the resistance in both air and the analytic gas are under grain boundary control that means no dependence on D. In another case, as D decreases below 2L, the resistance in the analytic gas is under grain control while the resistance in the air is still under grain boundary control, sensitivity ($S = \frac{R_g}{R_a}$) has a trend of increase. Thus, when the grain size of metal oxide particles reaches the nano-scale, higher sensitivity may be attained by means of grain size reduction. [24]

1.4 Tungsten trioxide (WO_3) as a selective NO sensor

The crystal structure of WO_3 is a distortion of rhenium oxide cubic structure in which tungsten atoms are located in cube corners and the oxygen atoms are located on the cube edges [25]. Each tungsten atom is surrounded by six oxygen atoms, forming an octahedron. The slight rotation of these octahedral with respect to each other, as well as unequal bond lengths in the octahedral coordination, causes lattice distortion and reduces the symmetry. The distorted structure is stable in several forms giving rise to different phases depending on the temperature. Figure 1 (adapted from [26]) shows the 7 known polymorphic transformations of WO_3.

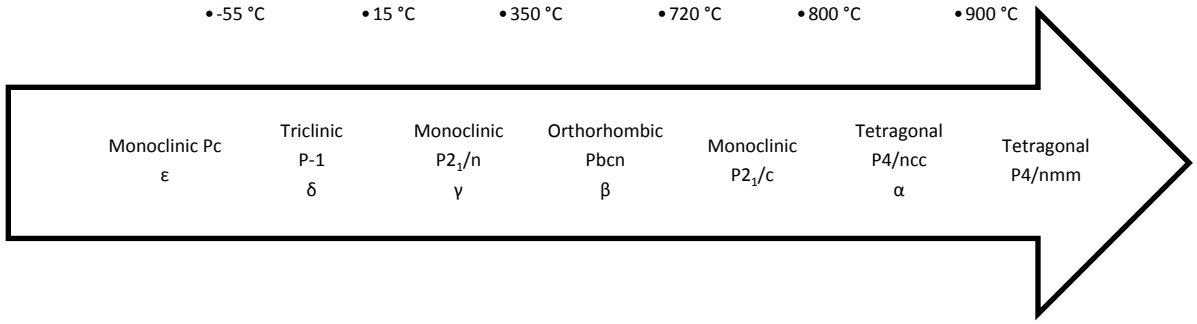

Figure 1 Phase transformations in WO_3

In 1991, Yamazoe et al. [27] first discovered the sensing properties of WO_3 towards NO and NO_2. The sensitivity towards 200 ppm NO and 80 ppm NO_2 was 31 and 97 respectively at 300 °C. This research marked the beginning of a new era for NO sensing, after which many studies were focused on this specific topic by using different methods to produce WO_3 sensors.

Earlier work by our group [28] introduced the polymorph-gas selection map of resistive gas sensors by studying tungsten oxides and molybdenum oxides. It provides the direction to develop chemo-resistive gas sensors by size control and operation temperature selection so as to attain the polymorph required for the gas tested.

Penza et al. [29] used radio frequency sputtering system to produce WO_3 film. The substrate they used was a 15×15 mm glass whose thickness was 5mm. The thickness of films produced varied from 500 to 5000 Å according to the deposition time and input power that changed between 100 and 300 W. The films were annealed at 400 °C in dry air for at least 6 hours to stabilize the sensing properties. They compared the XRD results from two films with different grown rates, the phase of both were tetragonal and it showed that the film deposited at lower rate had a better structural quality. They found out the optimum operating temperature was 250 °C after testing the sensing with NO_x, NH_3, H_2, H_2S, SO_2, CO_x and CH_4. The sensor showed good selectivity of NO_x against other gases. The threshold limit of the sensor at 250 °C for NO_2 and NO was 2 and 500 ppm.

Polleux et al. [30] used tungsten isopropoxide and benzyl alcohol to build a versatile reaction system for the preparation of crystalline tungsten oxide nanowires performed in a glass beaker at low temperature. The length of the nanowire bundles ranged from 300 to 1000 nm and the width was between 20 and 100 nm. The diameter of all nanowires was very uniform being in the range of (1±0.1) nm and they were mostly oriented parallel to each other with an equal distance. To make a stable sensor, a suspension of the tungsten oxide nano-bundles in ethanol was drop coated onto the aluminum substrate and then the sensor was heat-treated at 500 °C to be stabilized. The sensor showed high sensitivity (≈9) at very low concentration of NO_2 (about 500 ppb), which might be attributed to the high surface area and high crystallinity with appropriate porosity of the nanowire film. The response of the sensor to NO_2 decreased with increasing temperature and almost lost their sensitivity at 300 °C higher than which it could still be sensitive to reducing gases such as hydrocarbons and volatile organic compounds.

Wang [31], a former member of our group, built a prototype breathalyzer to detect acetone in human breath for diagnosing diabetes. The sensor was made of ε-tungsten trioxide, which is selective to acetone at the operating temperature. The concentration of gases tested in the study was down to 200 ppb and it showed adequate selectivity at the threshold concentration (1.8 ppm) of diabetes diagnosis. It was suggested that the acentric structure of ε-tungsten trioxide played an important role in the selective detection of acetone that has a high dipole moment than any other gases tested.

Marquis and Vetelino [32] tried to build a sensor arrays for fossil burning gases emission. They controlled substrate material, film thickness, film doping, deposition temperature and operation temperature in radio frequency sputtering to produce tungsten trioxide gas sensor. They chose 1000 Å WO_3 un-doped film sputtered at 400 °C on sapphire operating at 300 °C as NO_x sensor and 5000 Å WO_3 film co-sputtered with 16 Å Au at 200 °C on alumina operating at 350 °C as NH_3 sensor after a large number of tests. The response time for the NH_3 film ranged from 7 min for 1 ppm NH_3 to about 4 min for 50 ppm NH_3 and the response time for the NO_x film ranged from about 6 min for 1 ppm NO_x to less than 2 min for 75 ppm NO_x. They also tested the short and long-term stability of each film exposed to 15% relative humidity in the air. The baseline variation was in 3% over a 3 min period and in 8 % over a 10-hour period for the NH_3 sensor while the short-term stability of NO_x film was in less than 0.6 % and the long-term stability was about 20 %. The sensor array showed good selectivity to 10 ppm NH_3 and 75 ppm NO_x and H_2S that is a gaseous emission in fossil burning systems.

Lee et al. [33] made NO_x sensors with TiO_2 doped tungsten trioxides by sol-coprecipation of WCl_6 and $TiCl_4$ solution with ammonium hydroxide and surfactant and screen-printing after calcination at high temperature. The grain size of TiO_2 doped WO_3 was smaller than pure WO_3

or the simple mixture of WO_3 and TiO_2 powder. The TiO_2 doped WO_3 showed excellent sensitivity to low concentration of NO_x (0.5-30 ppm), short response time (1-2 min) and short recovery time (2-3 min) at 350 °C which was the optimum temperature for NO_x testing. It was illustrated that the size effect introduced by TiO_2 enhanced the sensing performance of WO_3.

In the study of Yu-De et al. [34], The electrical and gas-sensing properties of calcined tungsten trioxide were investigated. WO_3 with SiO_2 (4 wt. %) were fabricated on an alumina tube with Au electrodes and Platinum wires. A Ni-Cd alloy crossing alumina tube as a resistor was used for the heating. The sensors were calcined at different temperatures (350-800 °C) and then were aged at 250 °C for 150 hours in air to improve the stability and repeatability. When operating at the same temperature (200 and 250 °C), sensors that were calcined at higher temperature had smaller resistance baseline. It was showed that the sensor had best thermal stability in the operating temperature range of 175 to 225 °C, where the resistance was low and had little variation. By testing the sensitivity of the sensors to different gases, such as ethanol, petrol, methane and butane, at different calcining temperature, the optimum one was 500 °C. The sensor showed highest sensitivity (about 40 at 80 °C) to ethanol (100 ppm) among those gases tested. At calcining temperature of 500 °C and operating temperature of 200 °C, the WO_3 gas sensors which were compounds of monoclinic and triclinic phase (by XRD results) had good thermal stability and good sensing properties to ethanol.

Yin et al. [35] prepared Au-modified WO_3 nanocomposites by chemically reducing $HAuCl_4$ on the surface of two-dimensional WO_3 nanoplates, which were made by intercalation-topochemical process. WO_3 with 1 wt. % Au showed best sensing performance at 170 °C to NO (0.5-10 ppm), which was higher than that of pure plate like WO_3. It showed high selectivity to

NO among various inorganic gases (H_2, SO_2, and CO) and volatile organic compound (ethanol, acetone, methanol and benzene) at temperature lower than 200 °C.

Ponzoni et al. [36] prepared WO_{3-x} nanowires by thermal evaporation of tungsten powders at 1400-1450 °C in oxygen for 10 minutes. The width of the nanowires ranged from 0.7 to 200 nanometers and a 3D networks was formed by nanowires intercrossing each other. After the nanowire networks were drop coated onto alumina substrates and annealed in air at 300 °C for six days for stabilization, the sensors were measured for the response towards NO_2, H_2S, CO and NH_3. The sensor had excellent response (about 6) to NO_2 at low concentration (50 ppb) at 300 °C. The sensor was found to have better response intensity but longer response and recovery time at lower temperature (more than 40 minutes at 200 °C) at the testing range of 100-500 °C for NO_2. It appeared that the optimum temperature for sensing was 300 °C to achieve the balance between response intensity and dynamics. They also found that the sensor had weak responses towards NH_3 and CO at any working temperature, which was evidence for the good selectivity for the WO_{3-x} nanowire systems being good NO_2 sensor.

Kim et al. [37] made gas sensor by drop coating $WO_{2.72}$ nanorod solution on the Si bulk-micromachined membrane with a hotplate for temperature control. The resistance of the sensor decreased when exposed to 100 ppm ammonia (NH_3) at the temperature range of 150-250 °C but increased at temperature lower than 70 °C. Further sensing tests to gases like 2% N_2 (or air), 1000 ppm ethanol, 10 ppm NH_3 and 3 ppm NO_2 were performed at room temperature. All of them had increase in resistance except for N_2 that had little change and their response sensitivity ascended in the order of air, ethanol, ammonia and nitric dioxide when the recovery time ascended in the opposite sequence.

In the dissertation of one of our former group member Prasad [38], he used acid precipitation route to produce tungsten oxide thin films. Two different phases (orthorhombic and monoclinic phases) were obtained by calcination at different temperature. Phase transformation from monoclinic to orthorhombic was found to occur in the temperature range of 350-400 °C. The sensing test was performed at the temperature range of 200-500 °C to nitrogen dioxide and ammonia and it was found that both phases of WO_3 had good selectivity of nitrogen dioxide against ammonia and monoclinic phase WO_3 had best sensing performance to nitrogen dioxide in the temperature range of 200-300 °C.

Krithika [39] used sol-gel method to prepare WO_3 nanoparticles and thin films of WO_3 were prepared by spin coating and drop coating of the prepared sol on the 3 mm × 3 mm Al_2O_3 substrates. The films attained were then calcined at 400 °C for 6 hours and 515 °C for 8 hours to get monoclinic and orthorhombic phases respectively according to the result from differential scanning calorimetry (DSC) test. The average grain size of the particles which calcined at 400 °C was around 10-20 nm. WO_3 with either monoclinic or orthorhombic phase was tested for the response to NO_2, isoprene, acetone and ethanol at different ppm levels at 400 and 500 °C in respect. It showed that the monoclinic phase showed no cross-sensitivity toward reducing gases like hydrocarbons and VOCs while the orthorhombic phase had higher sensitivity for similar concentration of NO_2 but cross-sensitivity towards reducing gases. She also tested sensing using both polymorphs for ppb level sensing of NO and NO_2 at 400 and 200 °C for monoclinic and orthorhombic phase respectively. The sensitivity of the monoclinic phase for NO was a little greater than NO_2 at the same concentration while the sensitivity of the orthorhombic phase to NO_2 was much higher than NO.

In the conclusion of her thesis, that author suggested that the similarity of sensing response to oxidizing gases like NO and NO_2 of both monoclinic and orthorhombic phases was because they were isostructural and the mechanism of such sensing was absorption based that didn't affect the bond on the metal oxide surface. However the sensing behavior towards reducing gases was different. 'Magneli phase' or crystallographic shear (CS) planes existed in orthorhombic phase which played a critical role in inserting oxygen in to the hydrocarbon molecule as catalysts for selective oxidation. The sensing mechanism of such kind was reaction based. Two different sensing mechanisms exhibit from two polymorphs that are isostructural.

Wang [40], in his dissertation, used flame spray pyrolysis method to synthesis ε-WO_3. The percentage of ε-WO_3 was related to the particle size of the particles and the smaller they are the higher percentage of ε-WO_3. However, after calcination with as-received WO_3 the ε-WO_3 vanished. So he came up with an idea of doping chromium in the material by forming a surface layer, which could prevent the ε to γ transition. The WO_3 with 10 at% Cr doped sensor was found to have good sensitivity and selectivity to low concentrations of acetone (from 0.2 to 1 ppm) compared to other interfering gases at 400 °C. The mechanism behind the high sensitivity to acetone of ε-WO_3 was believed to related to the surface dipole of ferroelectric ε-WO_3 and the highly polar acetone gas molecules.

1.5 Processing of NO sensing elements

Recent reports in the sensor literature have adapted many different ways to produce sensing materials. Here are three of the most applicable methods so far.

1.5.1 Sol-gel

Sol-gel process [41] involves solid nanoparticles dispersed in a continuous liquid (sol) which agglomerate to form interconnected three-dimensional solid state network with isolated liquid phase (gel). This is a relatively inexpensive method and could be easily applied in the lab. The starting materials for sol are usually inorganic metal salts or organic metal compounds. The versatility of the sol-gel process is manifested in the very many ways which could be applied to attain the final products depending on the application requirements, such as spin coating, drop coating, electrospinning.

Krithika [42] prepared nanostructured WO_3 using sol-gel method and spin coated on aluminum substrates. After heat treatment at 400° for six hours, the amorphous phase turned into monoclinic phase by XRD result and Raman spectrum. The sensor was tested to nitric oxide, acetone, carbon monoxide, ethanol, isoprene and methanol, showing a good selectivity for nitric oxide against other gases. Also, the concentration of nitric oxide was down to 300 ppb, which is relevant to those found in human breath level. With that being tested, the materials could be a good prospect for human breath nitric oxide detection.

1.5.2 Electrospinning

Electrospinning is an easy to go way to produce nanofiber. It uses electrical charge to extract fine fibers from liquid to deposit on the charged substrate. The basic setup for electrospinning usually consists of syringe pump, needle that is connected to power supply and grounded substrate. There are many parameters controlling the outcome of the fibers: the properties of the solution (viscosity, surface tension and conductivity), potential of the charge, flow rate, distance between needle and substrate, ambient atmosphere (temperature, humidity and air flow).

Former group members, Sawicka and Prasad [43] combined metal oxide sol-gel and polymer to prepare the precursor for electrospinning and they focused on the MoO_3/WO_3 and polyvinylpyrrolidone (PVP) system. Compared with the sol-gel prepared films, the nanowires of WO_3 showed better sensitivity, fast response and lower sensing limit to nitrogen dioxide. However, the range of concentration was from 50 to 500 ppm, which is too high for human breath sample.

1.5.3 Flame spray pyrolysis (FSP)

To produce nano-sized particles with high purity and good thermal stability in a scalable way, scientists came up with the idea of using flame in gas phase process. Compared to those wet phase process mostly used, which involves redundant moves like filtration, drying, calcination, etc., gas phase process is easier to control and ecofriendly because of water saving, just named a few advantages here.

Flame synthesis of materials doesn't need extra sources of energy from the system to converse the precursor and the energy for the particles formation is coming from the in-situ chemical reaction of the precursor in the synthesis process. Various reactors and methods have been adapted to produce different kinds of metals and metal oxides. According to the precursor state fed into the system, the flame synthesis process could be classified to two main categories: vapor-fed aerosol flame synthesis (VAFS) and liquid-fed aerosol flame synthesis (LAFS).

a) Vapor-fed aerosol flame synthesis is the pyrolysis of volatile precursors in flames. The particles form by nucleation in the gas phase after conversion of volatile precursors and grow by surface reaction and/or coagulation and coalescence into larger particles. The limitation of VAFS

is the lack of available volatile precursors at reasonable price in the market. Fumed silica, alumina and pigmentary titania have been already produced by VAFS. [44]

b) Liquid-fed aerosol flame synthesis is more versatile because the precursor doesn't have to be volatile. In this case, the liquid precursor is sprayed by air-assisted atomization and vaporized to form particles. Complete vaporization leads to formation of nanoparticles like VAFS but incomplete vaporization leads to micron-sized shell-like or hollow particles. Depending on the enthalpy content of the precursor and whether an extra flame is used as heat source to evaporate the precursor, liquid-fed aerosol flame synthesis could be classified to flame spray pyrolysis (FSP) and flame assisted spray pyrolysis (FASP). [44]

In FSP, metal organic precursor is dispersed by gas convection through a nozzle forming fine spray then ignited, vaporized and particles are formed by nucleation and grow from the gas phase. Because of the high maximum temperature and short residence time, the particles could be nano-sized and homogeneously formed; the schematic is shown as Figure 2. [45]

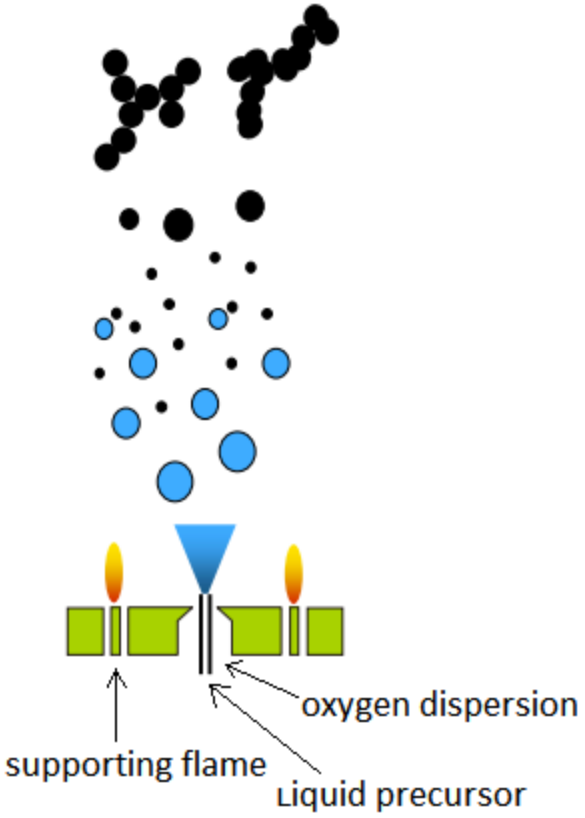

Figure 2 Schematic of FSP process

The as-prepared particles in flame synthesis process could be collected by filters, electrostatic precipitators or cyclones. Alternatively, a major advance of phase synthesis compared to wet-phase method is direct deposition on the substrate. The thickness and morphology of the materials on substrate could be reproduced and well controlled by this method. [46]

1.6 Statement of the research

Portable human breath detector is the future of medial devices for early and non-invasive disease prediction and monitoring. Chemical sensing is proven to be the most hopeful prospect for this purpose because of the small size, quick response, easy process and low price to fabricate.

Tungsten oxide sensors have been studied for the past decade on different kinds of gases because of the intrinsic properties of tungsten oxide, which exists as different phases in different environment, and many other materials have been studied for sensing of nitric oxide because of its unique guidance for disease in human breath.

In this thesis, the focus is on using flame spray pyrolysis to produced nano-sized tungsten trioxide particles and to test the sensing ability towards nitric oxide at low concentration that are relevant to human breath level.

Chapter 2 Experimental details

In this chapter, all the details of the experiment part of the thesis are presented. In the first part, raw materials synthesis using flame spray pyrolysis is discussed. Secondly, different materials characterization methods, including x-ray diffraction (XRD), scanning electron microscopy (SEM), transmission electron microscopy (TEM) and Raman spectroscopy are introduced. The last part describes the sensors preparation and sensing test setup.

2.1 Materials synthesis by flame spray pyrolysis (FSP)

The materials were synthesized by flame spray pyrolysis method using lab-scale nanopowders production system from Tethis (NP10) in our lab. The NP10 system contains of 3 main parts: nozzle unit, dispensing system and control unit, which are all located in the lab vented fume hood. The system is controlled by a computer, which guarantees the safety and accuracy of the synthesis process. A collecting system is based on glass fiber filters on the top of the collecting chamber

The precursor solution using in this thesis is prepared in this way: 0.3 M of tungsten (VI) isopropoxide (99%, All-Chemie) was dissolved in 2-propanol in nitrogen atmosphere glove box. After aging for a day, the precursor was supplied at a rate of 5 ml/min through the flame nozzle and dispersed by oxygen with a rate of 5 slm (standard liter per minute) to form fine spray. The fine spray was ignited and supported by the flame that was combustion of methane and oxygen at the rate of 1.5 slm and 3.0 slm respectively. The synthesized particles were deposited beneath the glass fiber filter (Whatman) and collected after the process was done. This part was carried out by my colleague Jusang Lee.

2.2 Materials characterization

2.2.1 X-ray diffraction (XRD)

X-ray diffraction is a non-destructive and flexible technology to reveal the chemical composition and crystallographic structural information of the materials.

Here is a famous equation called Bragg's Law:

$$2d \sin\theta = \lambda$$

When a monochromatic x-ray beam with wavelength λ is projected through a crystalline material with adjacent plane distance d at an angle θ. Only when the difference of distance travelled by the rays reflected at successive planes is a complete number n of wavelength of the beam, the diffraction happens. By varying the angle θ in a specific range, the Bragg's Law condition is satisfied by different d. A pattern of such material could be plotted by the resultant intensities of the diffracted peaks of radiation collected and the angular positions.

The XRD used in this research is Rigaku's Ultima III in BNL and it was operated at 40 kV and 30 mA. The 2θ ranges from 20° to 80°and the λ of this device is the wavelength of Cu Kα radiation that is 1.54184 Å. The d values of the peaks in the plot could be compared with standard Joint Committee on Powder Diffraction Standards (JCPDS) data to identify the specific phases in the material. This part was carried out by my colleague Shantanu Sood.

2.2.2 Scanning and Transmission electron microscopy (SEM/TEM)

Scanning electron microscopy is a type of electron microscopy using electrons rather than light to produce high-resolution images of sample surface. The image from SEM could have high depth of field to show three-dimensional view of the sample surface.

In SEM, a beam of electrons is produced by heating up the tungsten filament or by field emission at the top of the chamber of the microscope. The electrons go down vertically through the electromagnetic lenses, which focus the beam down to a point on the sample, in the chamber. Once the electrons hit the sample, other electrons (back-scattered or secondary) are ejected from the sample collected by the detectors above the sample. The beam of electrons scans a specific area on the sample and detectors synchronously collect the back-scattered or secondary electrons and convert them to signals to the system so we can see the image on the screen.

Transmission electron microscopy is another type of electron microscopy. It could produce images with even higher resolution and get the electron diffraction patterns of the sample at the same time.

The beam of electrons is produced in the same way as SEM, but the sample is very thin that the electrons go through instead of reflecting back from the surface. Some beams go through the sample (direct beam), while others undergo Bragg diffraction by the scattering planes of atoms and converge on the back focal plane. If the object plane of the imaging lens is adjusted to coincide with the image plane of the objective lens, an image of the sample's morphology would appear on the screen. If the object plane of the former lens is adjusted as the same as the back focal plane of the latter, the diffraction pattern would show on the screen thus providing structural information about the sample.

The TEM using in this research is JEOL's JEM-1400. This part was carried out by my colleague Shantanu Sood.

2.2.3 Raman Spectroscopy

Raman spectroscopy is a technique of light scattering, which can be thought of as a process where a photon of light interacts with a sample to produce scattered radiation of different wavelengths, in a very simple way.

When light interacts with a sample it may be reflected, absorbed or scattered in some manner. If the frequency of the scattered radiation is analyzed, those radiations with the same wavelength as the incident radiation is called Rayleigh scattering and those radiations with different wavelength is called Stokes and Anti-Stokes Ramen Scattering.

The incident protons interact with the present molecule and the energy change of a photon is characteristic of each bond present. By such a way, scientists build a table of Raman band positions, thus a range of wavelengths associated with different bonds and vibrations could be the fingerprint of different molecules.

The Raman spectroscopy using in this research is WiTec Alpha combination microscope for atomic force microscopy, scanning near-field optical microscopy, confocal microscopy, and confocal Raman microscopy within the same field of view. The laser excitation source is the 532nm wavelength one. This part was carried out by my colleague Wen Ling Liao.

2.3 Sensor preparation

To prepare the gas sensor, 0.05 g of the as-received WO_3 powders were dissolved in ethanol and the solution was ultrasonically stirred for 15 minutes. Then 15 drops of the solution was deposited on a platinum electrode-coated 3×3 mm^2 Al_2O_3 substrate (Figure 3). The substrate was dried after every drop at 100 °C for 5 minutes. After the materials was uniformly deposited onto the substrate, the substrates was heat treated at 500 °C for 8 hours to stabilize the phase.

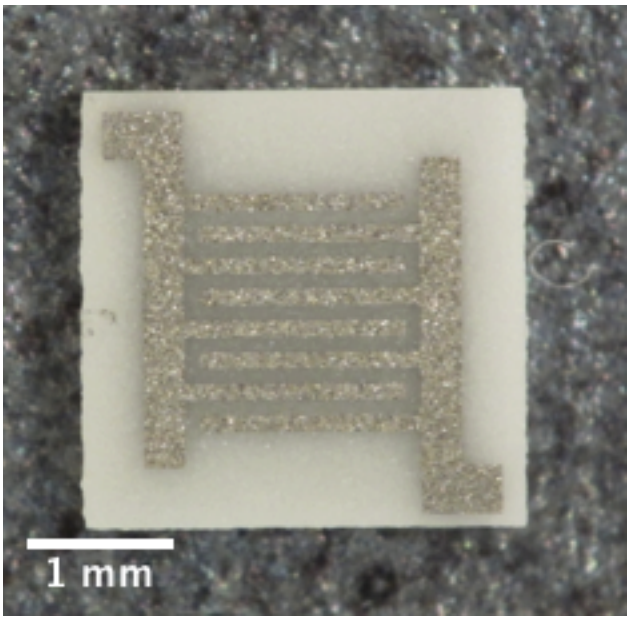

Figure 3 Al_2O_3 substrates

2.4 Sensing test setup

The as-prepared sensor is put into a quartz tube and connected with measuring circuit with gold wire (Alfa Aesar, 0.25 mm diameter, 99.998%) welded on the integrated platinum circuits on the substrate, and the glass tube was put inside the tube furnace (Lindberg/Blue). The resistance was recorded by software (Agilent Digital Multimeter Connectivity Utility) on the computer.

The gases used were UHP Nitrogen and Oxygen, 10 ppm nitric oxide in nitrogen background (Global Calibration Gases). The concentration of nitric oxide in the mixed gas flow was controlled by varying the flow rates of the nitric oxide and background air (nitrogen and oxygen). The flow rates of the gases were controlled using the gas flow bench by a 247-MKS 4-channal readout and 1479 MKS mass flow controllers in the unit of stand cubic centimeter per minute (sccm).

The schematic of the sensing setup is showed in Figure 4.

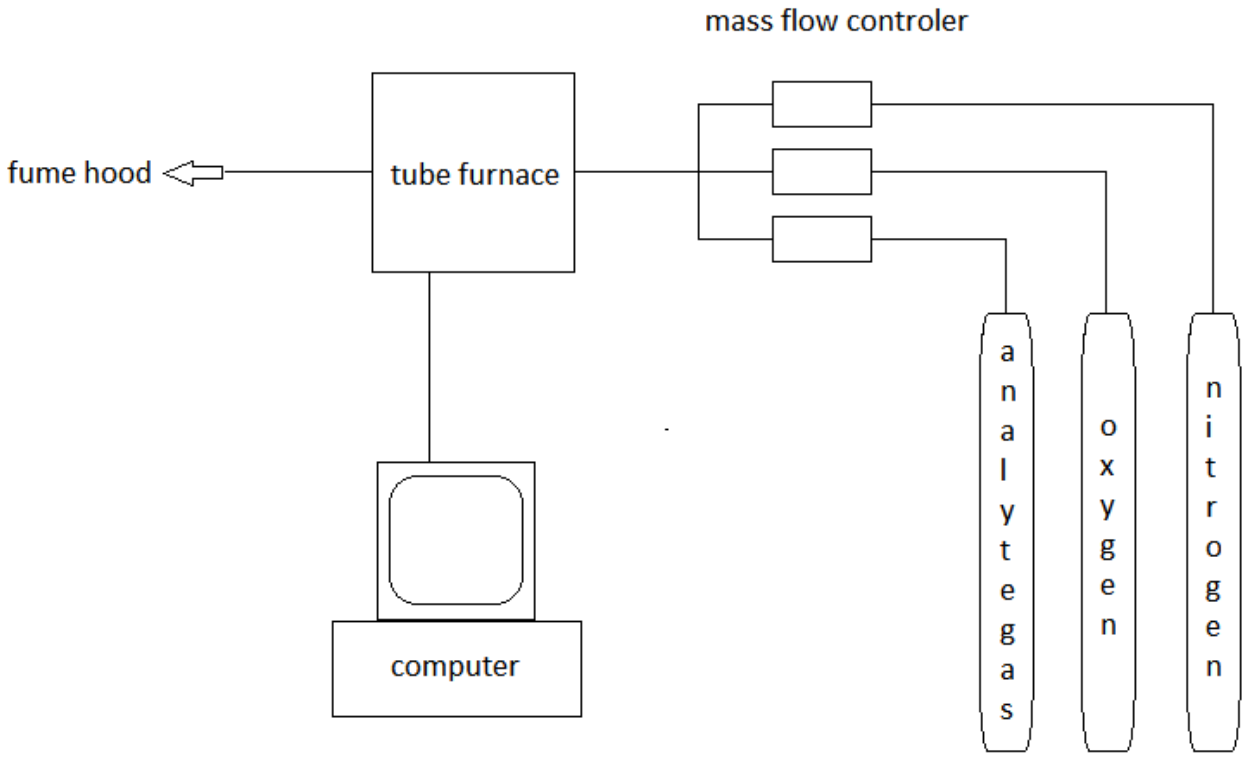

Figure 4 Schematic of the sensing setup

Chapter 3 Experiment results

3.1 Structure and morphology

3.1.1 X-ray diffraction

Figure 5 gives the profile of the XRD results of WO_3 treated at four different temperatures: room temperature, 200 °C, 350 °C and 500 °C. The main peaks in the sample heat-treated at 500 °C can be indexed to the JCPDS card number 83-0950. From the result by XRD, the phase in the sample at 500 °C is mostly monoclinic phase (space group: $P2_1/n$, lattice parameters: a=7.301 Å, b=7.538 Å, c=7.689 Å, β=90.893°).

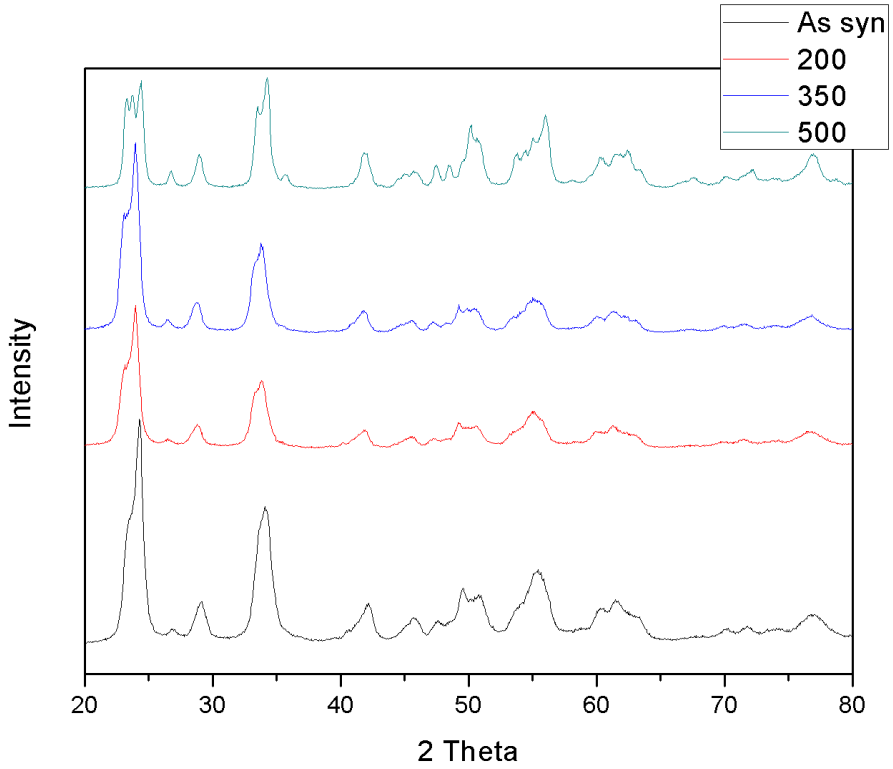

Figure 5 XRD results profile of WO_3 at different temperatures

3.1.2 Transmission electron microscopy

TEM analysis were carried out for the sample after 500 °C heat-treatment, as shown in Figure 6. The grain size of the particles ranges from 20 to 40 nm. The agglomeration of the particles is not that strong as the particles prepared by sol-gel methods [39], which is a benefit of rapid quench process of FSP method.

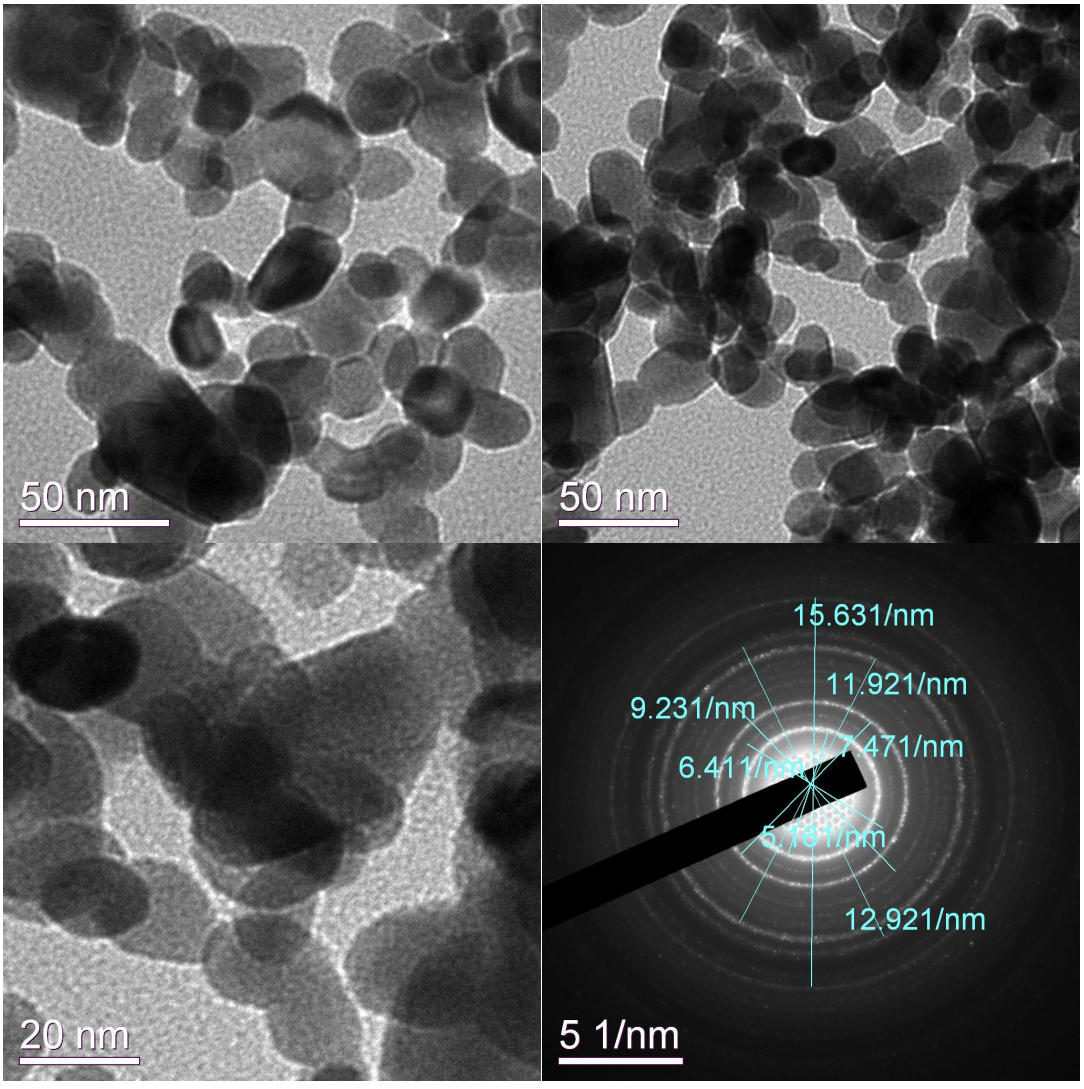

Figure 6 TEM images of 500 °C heat-treated WO_3 at different spots of one sample and selected area electron diffraction (SAED) pattern of the sample

From the SAED pattern Figure 6, the interplanar spacings correspond to those of monoclinic WO_3 (JCPDS card number 83-0950), which is in accordance with the results from

XRD. Also, the sharp rings in the SAED pattern indicates the nanoparticles are polycrystalline and well crystalized.

3.1.3 Raman spectroscopy

Figure 7 shows the Raman spectra of the WO_3 particles heat-treated at 500 °C. It presents the typical structure of crystalline WO_3 structure with three main regions at 900-600, 400-200 and below 200 cm^{-1}.

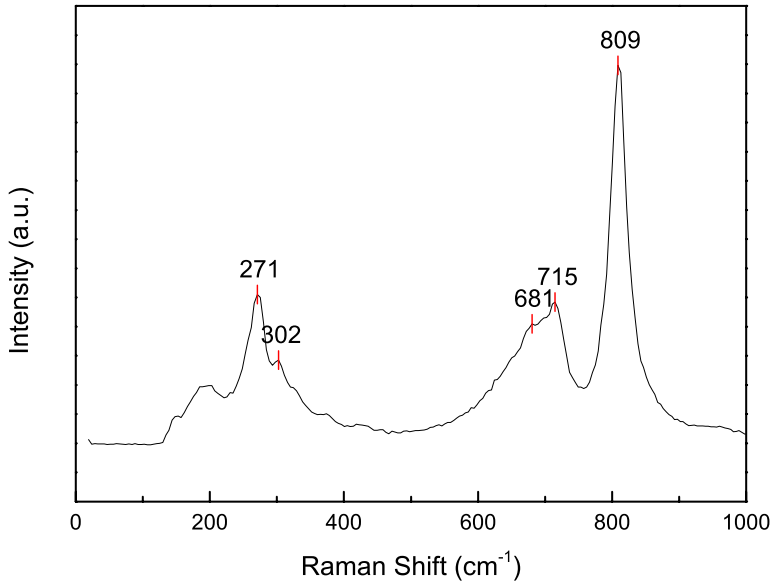

Figure 7 Raman spectra of WO_3 annealed at 500 °C

Compared to Wang's dissertation [40], the peaks found in Figure 7, such as 271, 715, and 809, fit the monoclinic γ phase.

3.2 Sensing properties

The sensor response to different gases at 350 °C is shown in Figure 8. The gases tested are nitric oxide, ammonia, isoprene and acetone (background gas: 80% nitrogen and 20%

oxygen). The concentration is 2 ppm of each gas. As seen from the figure, the sensor response to nitric oxide is in the opposite way as the others (resistance increase) as expected for an n-type semiconductor responding to an oxidizing gas and it's strong and fast (the reason for the increase of resistance for ammonia at the very beginning when gas was introduced might be unstable electric contact of the measurement).

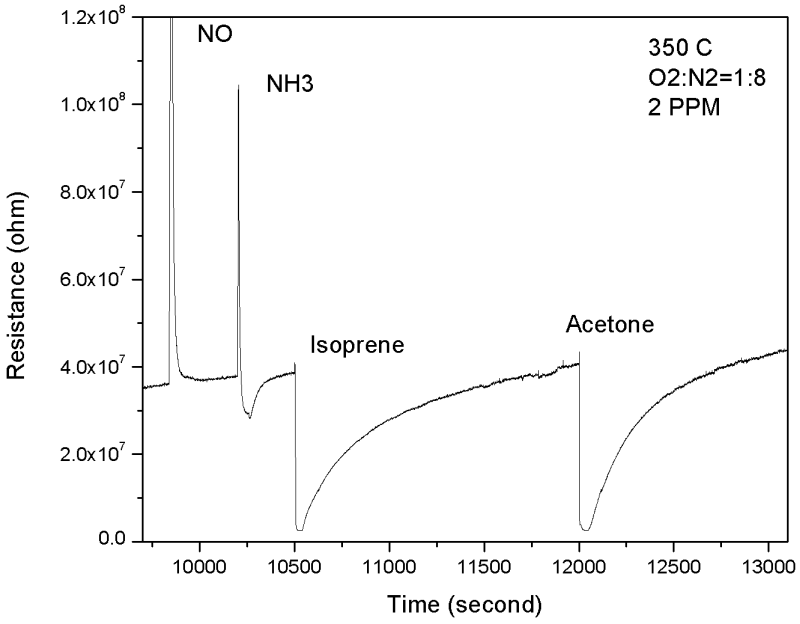

Figure 8 Sensing results at 350 °C against nitric oxide, ammonia, isoprene and acetone

Figure 9 and Figure 10 show the sensing results at 350 °C and 200 °C respectively. The pulse for NO is 30 seconds each time. The sensitivity is calculated in Table 1. The lower the temperature, the better the sensitivity for the WO_3 sensor. However, the time for the sensor resistance to get back to the baseline after NO was off is longer at lower temperature, which was about 5 minutes at 200 °C compared to about 3 minutes at 350 °C.

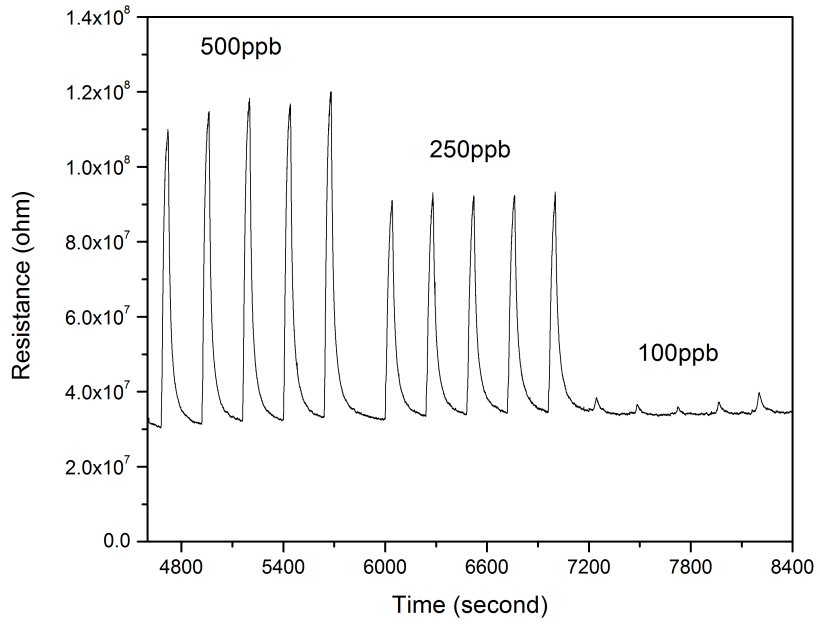

Figure 9 Sensing result at 350 °C

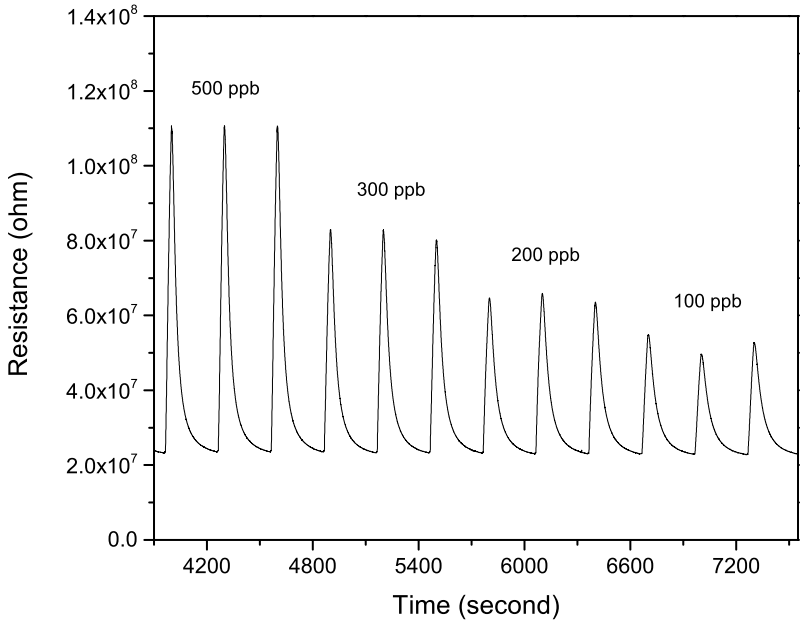

Figure 10 Sensing result at 200 °C

Table 1 Sensitivity at 200 °C and 350 °C

Temperature (°C)	200				350		
Concentration (ppb)	500	300	200	100	500	250	100
Sensitivity ($S_n = \frac{R_g - R_a}{R_a}$)	3.8	2.5	1.8	1.2	2.6	2	0.2
Sensitivity ($S = \frac{R_g}{R_a}$)	4.8	3.5	2.8	2.5	3.2	2.8	1.2

3.3 Discussion

From the above results, well defined and stoichiometry nano-sized WO_3 particles could be produced by FSP method in a single step. Nanoparticle based sensor showed good response to NO at two different temperature tested (200 and 350 °C).

As known from the literature, the sensor made by Ponzoni's team [36] had high content of oxygen vacancy thus a stoichiometry structure could not be reached. Also, the phase composition of WO_3 was unclear from their study.

By a direct comparison of the sensing performance, the sensitivity ($S = \frac{R_g}{R_a}$) of their sensor was about 6 in about **10 minutes** of NO_2 gas pulse at 300 °C with 50 ppb while the one in this work was about 2.5 and 1.2 in 30 seconds of NO gas pulse at 200 and 350 °C with 100 ppb

respectively. Because a single human breathe couldn't last for minutes, 30 seconds of gas pulse was therefore chosen instead of 10 minutes as in Ponzoni's work. Within such a short time, the sensor in our work showed similar sensitivity to the best result reported of a very long signal.

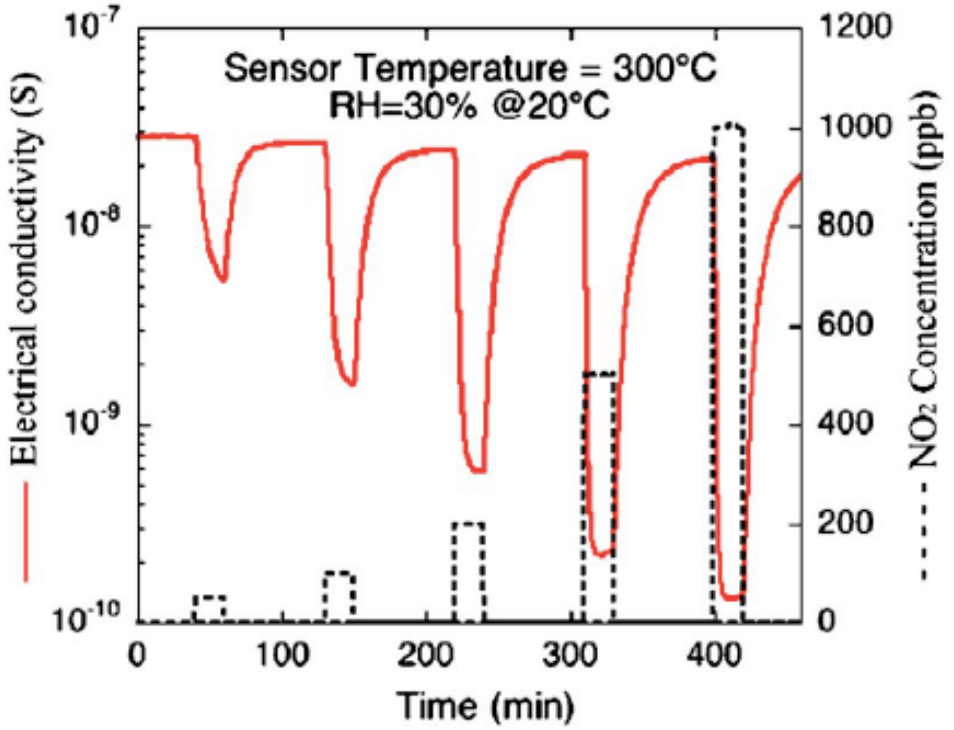

Figure 11 Sensor response of thermal evaporation made WO_3 to NO_2 of different concentrations, measured at 300 °C and 30% of relative humidity at 20 °[36]

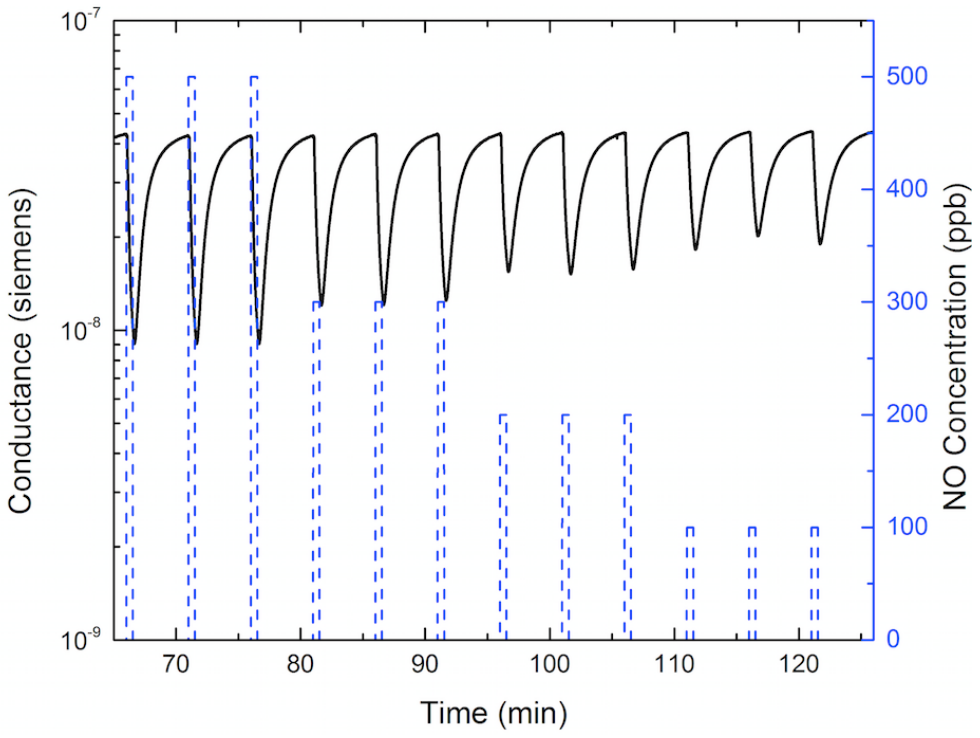

Figure 12 Sensor response of FSP made WO_3 to NO of different concentrations measured at 200 °C with nitrogen and oxygen as background gas

Comparing the sensor in this study with Krithika's WO_3 sensor [39], the effect of agglomeration was weaker (Figure 13 and Figure 14) which should be the benefit of rapid quench.

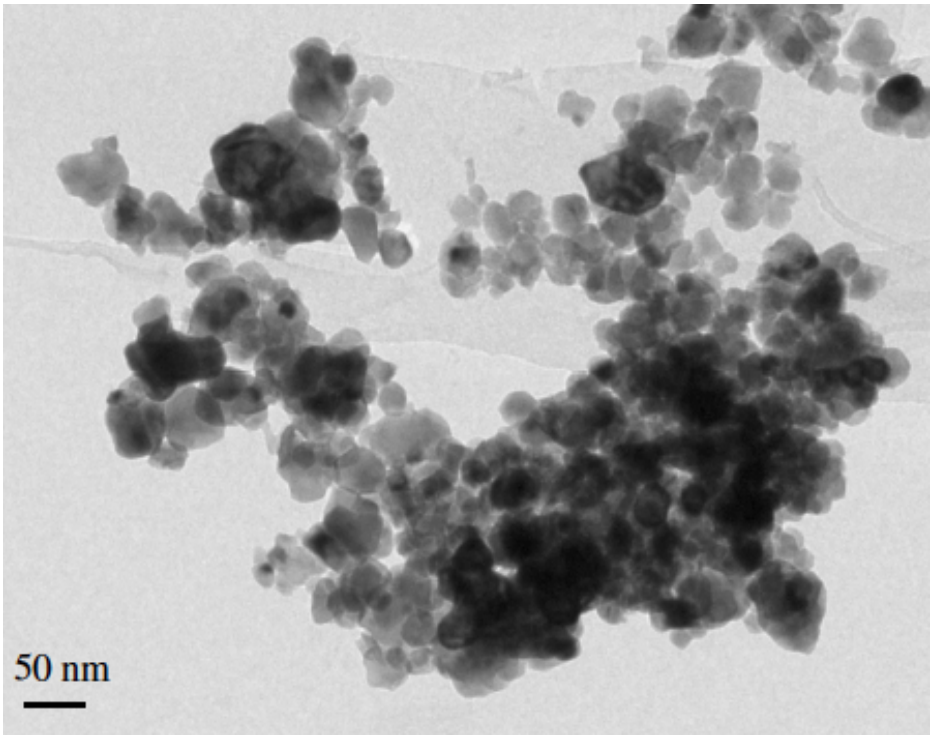

Figure 13 TEM view of the 515 °C annealed WO_3 by sol gel [39]

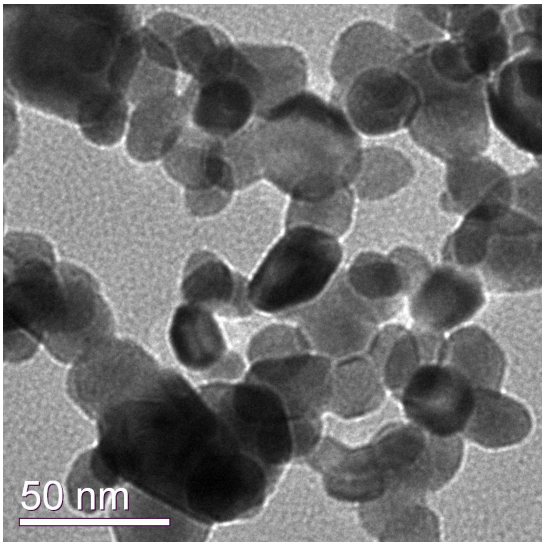

Figure 14 TEM view of the 500 °C annealed WO_3 by FSP

The sensing performance of monoclinic phase in her study was tested at 400 °C, as shown in Figure 15, and the sensitivity was plotted as Figure 16. Since she used $\frac{R_g}{R_a}$ as S, a sensitivity graph with this definition of S is plotted for direct comparison here as Figure 17. At

500 ppm level, the sensitivity of FSP made WO_3 based sensor is about 4.8 at 200 °C and 3.2 at 350 °C while that of sol-gel made WO_4 by Krithika is about 1.2 at 400 °C.

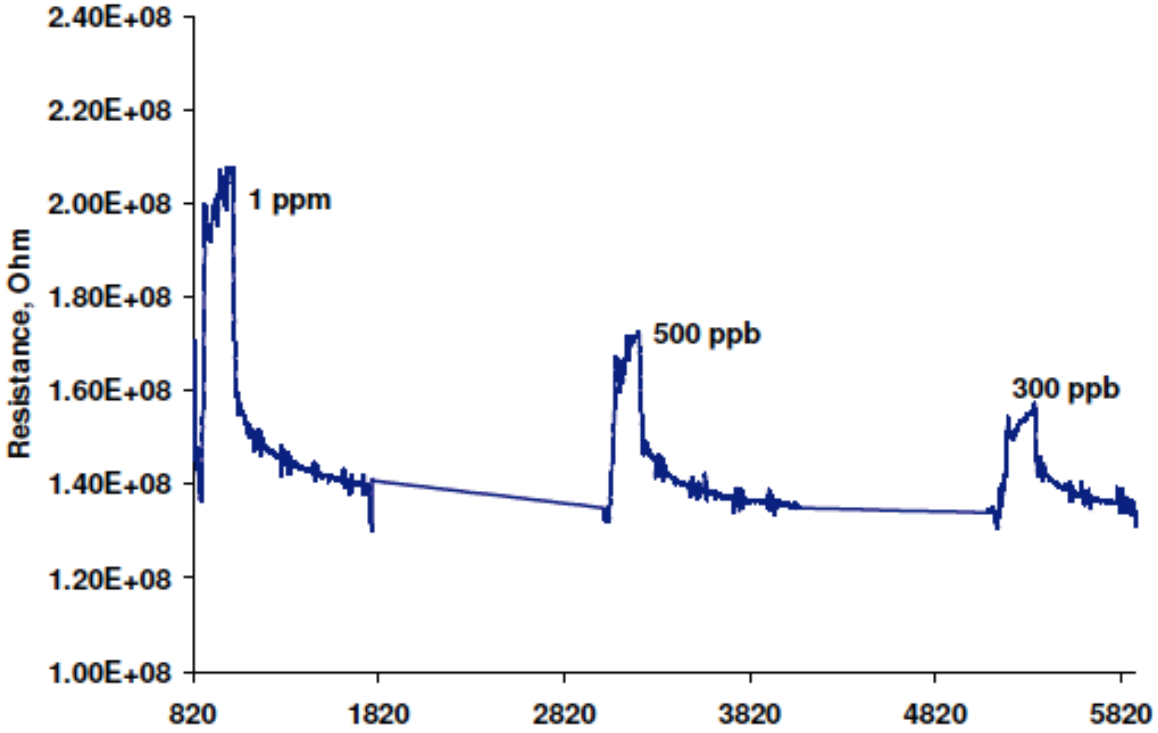

Figure 15 Sensing response of monoclinic polymorph at 400°C to NO [39]

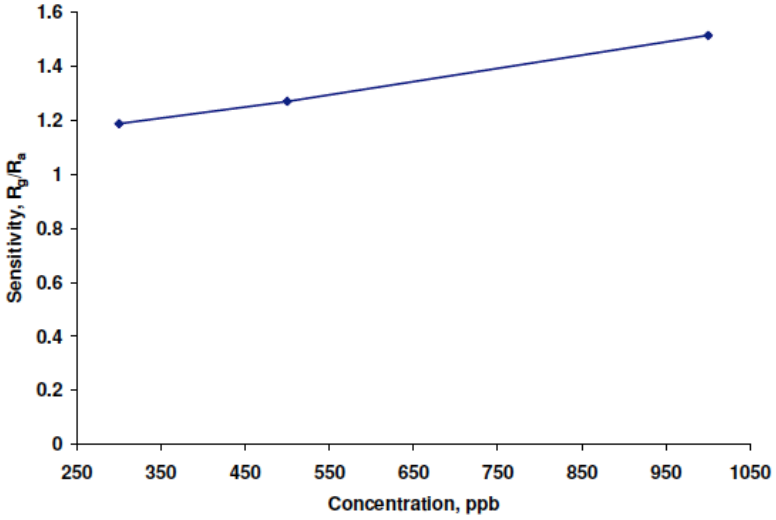

Figure 16 Sensitivity variation of the monoclinic phase sensor by sol-gel with NO concentration at 400 °C [39]

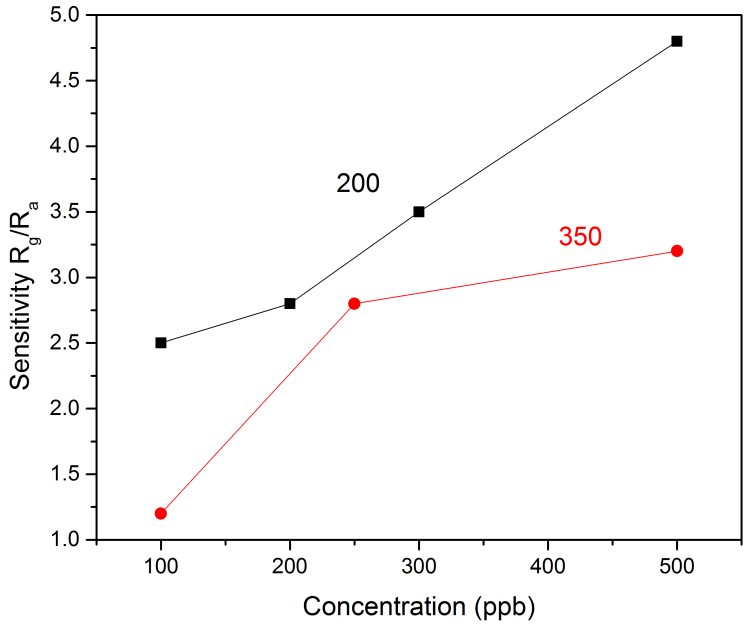

Figure 17 Sensitivity variation of the monoclinic phase sensor by FSP with NO concentration at 200 and 350 °C

Chapter 4 Conclusion and future work

4.1 Conclusion

This thesis has made a promising NO sensor from rapidly solidified WO_3 nanoparticles. The particles were synthesized by FSP method and heat-treated at 500 °C to stabilize the monoclinic phase (gamma phase). The sensor was made by drop-coating the particles on a 3×3 mm^2 substrate, and being measured in a tube furnace in the background gas of 80% nitrogen and 20% oxygen at 200 and 350 °C, in respect.

At 350 °C, the sensor showed good selectivity to NO and good response to NO at ppb level. The sensor behaved better sensitivity but slower recovery time at 200 °C, which is good for hand-held medical device affording lower power requirements and energy consumption.

Comparing with other NO sensors, FSP made one has the advantage of well-defined stoichiometry and high surface area because of lower degree of agglomeration. The FSP made sensor shows good sensitivity to NO at ppb level, plus it is easy to synthesize the nanoparticles by flame spray process to large amount, making it a notable way for gas sensor synthesis in the future.

4.2 Future work

The thickness of the particles layer on the substrate wasn't precisely controlled by drop-coating method in this research. Direct deposition by FSP method [46] might be a solution and study on thickness effects could be carried on.

The sensing measurement environment in the tube furnace is not the exact environment in practical use. The furnace not only heats up the sensor but also the gases, which might affect

the result of sensing. A new chamber with heater on the substrate is being developed and should be used in the future work.

The measurement of selectivity of the sensor is not complete at different temperature. And the sensor reproducibility needs to be tested in the future work.

Chapter 5 Bibliography

1. Hart, M.H., *The evolution of the atmosphere of the earth.* Icarus, 1978. **33**(1): p. 23-39.
2. Raven, P., et al., *Biology*. 2010: McGraw-Hill Education.
3. Smith, A.D., et al., *Diagnosing asthma - Comparisons between exhaled nitric oxide measurements and conventional tests.* American Journal of Respiratory and Critical Care Medicine, 2004. **169**(4): p. 473-478.
4. Studer, S., et al., *Patterns and significance of exhaled-breath biomarkers in lung transplant recipients with acute allograft rejection.* The Journal of heart and lung transplantation, 2001. **20**(11): p. 1158-1166.
5. Kharitonov, S.A. and P.J. Barnes, *Exhaled markers of pulmonary disease.* American journal of respiratory and critical care medicine, 2001. **163**(7): p. 1693-1722.
6. Risby, T.H. and S.S. Sehnert, *Clinical application of breath biomarkers of oxidative stress status.* Free Radic Biol Med, 1999. **27**(11-12): p. 1182-92.
7. Sawicka, K., P. Gouma, and S. Simon, *Electrospun biocomposite nanofibers for urea biosensing.* Sensors and Actuators B: Chemical, 2005. **108**(1–2): p. 585-588.
8. Karl, T., et al., *Human breath isoprene and its relation to blood cholesterol levels: new measurements and modeling.* J Appl Physiol (1985), 2001. **91**(2): p. 762-70.
9. Pacher, P., J.S. Beckman, and L. Liaudet, *Nitric oxide and peroxynitrite in health and disease.* Physiological reviews, 2007. **87**(1): p. 315-424.
10. Barnes, P.J. and M. Belvisi, *Nitric oxide and lung disease.* Thorax, 1993. **48**(10): p. 1034-1043.
11. Kharitonov, S. and P. Barnes, *Clinical aspects of exhaled nitric oxide.* European Respiratory Journal, 2000. **16**(4): p. 781-792.
12. McMaster, M., *GC/MS: A Practical User's Guide*. 2008: Wiley.
13. Blake, R.S., P.S. Monks, and A.M. Ellis, *Proton-transfer reaction mass spectrometry.* Chemical Reviews, 2009. **109**(3): p. 861-896.
14. Smith, D. and P. Španěl, *Selected ion flow tube mass spectrometry (SIFT-MS) for on-line trace gas analysis.* Mass Spectrometry Reviews, 2005. **24**(5): p. 661-700.
15. Narhi, L.O., *Biophysics for Therapeutic Protein Development*. 2013: Springer.
16. Griffiths, P.R. and J.A. De Haseth, *Fourier Transform Infrared Spectrometry*. 2007: Wiley.
17. Fried, A. and D. Richter, *Infrared Absorption Spectroscopy*, in *Analytical Techniques for Atmospheric Measurement*. 2007, Blackwell Publishing. p. 72-146.
18. Clough, P.N. and B.A. Thrush, *Mechanism of chemiluminescent reaction between nitric oxide and ozone.* Transactions of the Faraday Society, 1967. **63**(0): p. 915-925.
19. *Expanding the Vision of Sensor Materials*. 1995: The National Academies Press.
20. Adam, H., G. Stanisław, and I. Folke, *Chemical sensors definitions and classification.* Pure Appl. Chem, 1991. **63**: p. 1274-1250.
21. Seiyama, T., et al., *A New Detector for Gaseous Components Using Semiconductive Thin Films.* Analytical Chemistry, 1962. **34**(11): p. 1502-1503.
22. Moseley, P., *New trends and future prospects of thick-and thin-film gas sensors.* Sensors and Actuators B: Chemical, 1991. **3**(3): p. 167-174.
23. Sze, S.M., *Semiconductor sensors*. 1994: Wiley-Interscience.

24. Tamaki, J., et al., *Grain-size effects in tungsten oxide-based sensor for nitrogen oxides.* Journal of the Electrochemical Society, 1994. **141**(8): p. 2207-2210.
25. Buseck, P. and M.S.o. America, *Minerals and Reactions at the Atomic Scale: Transmission Electron Microscopy*. 1992: Mineralogical Society of America.
26. Gurlo, A., *Nanosensors: towards morphological control of gas sensing activity. SnO2, In2O3, ZnO and WO3 case studies.* Nanoscale, 2011. **3**(1): p. 154-165.
27. Akiyama, M., et al., *Tungsten Oxide-Based Semiconductor Sensor Highly Sensitive to NO and NO2.* Chemistry Letters, 1991. **20**(9): p. 1611-1614.
28. Gouma, P., A. Prasad, and K. Iyer, *Selective nanoprobes for'signalling gases'.* Nanotechnology, 2006. **17**(4): p. S48.
29. Penza, M., et al., *Tungsten trioxide (WO_3) sputtered thin films for a NO_x gas sensor.* Sensors and Actuators B: Chemical, 1998. **50**(1): p. 9-18.
30. Polleux, J., et al., *Template-Free Synthesis and Assembly of Single-Crystalline Tungsten Oxide Nanowires and their Gas-Sensing Properties.* Angewandte Chemie, 2006. **118**(2): p. 267-271.
31. Wang, L., et al., *Nanosensor device for breath acetone detection.* Sensor Letters, 2010. **8**(5): p. 709-712.
32. Marquis, B.T. and J.F. Vetelino, *A semiconducting metal oxide sensor array for the detection of NO_x and NH_3.* Sensors and Actuators B: Chemical, 2001. **77**(1): p. 100-110.
33. Lee, D.-S., et al., *Nitrogen oxides-sensing characteristics of WO_3-based nanocrystalline thick film gas sensor.* Sensors and Actuators B: Chemical, 1999. **60**(1): p. 57-63.
34. Yu-De, W., et al., *Electrical and gas-sensing properties of WO_3 semiconductor material.* Solid-State Electronics, 2001. **45**(5): p. 639-644.
35. Yin, L., et al., *Enhanced selective response to nitric oxide (NO) of Au-modified tungsten trioxide nanoplates.* Materials Chemistry and Physics, 2013. **143**(1): p. 461-469.
36. Ponzoni, A., et al., *Ultrasensitive and highly selective gas sensors using three-dimensional tungsten oxide nanowire networks.* Applied Physics Letters, 2006. **88**(20): p. 3.
37. Kim, Y.S., et al., *Room-temperature semiconductor gas sensor based on nonstoichiometric tungsten oxide nanorod film.* Applied Physics Letters, 2005. **86**(21): p. -.
38. Prasad, A.K., *Study of gas specificity in molybdenum trioxide/tungsten oxide thin film sensors and their arrays.* 2005.
39. Kalyanasundaram, K., *Biomarker sensing using nanostructured metal oxide sensors*. 2007: ProQuest.
40. Wang, L., *Tailored synthesis and characterization of selective metabolite-detecting nanoprobes for handheld breath analysis.* 2008.
41. Zha, J. and H. Roggendorf, *Sol–gel science, the physics and chemistry of sol–gel processing.* Advanced Materials, 1991. **3**(10): p. 522-522.
42. Gouma, P.I. and K. Kalyanasundaram, *A selective nanosensing probe for nitric oxide.* Applied Physics Letters, 2008. **93**(24): p. 3.
43. Sawicka, K.M., A.K. Prasad, and P.I. Gouma, *Metal oxide nanowires for use in chemical sensing applications.* Sensor Letters, 2005. **3**(1): p. 31-35.
44. Strobel, R. and S.E. Pratsinis, *Flame aerosol synthesis of smart nanostructured materials.* Journal of Materials Chemistry, 2007. **17**(45): p. 4743-4756.

45. Strobel, R., A. Alfons, and S.E. Pratsinis, *Aerosol flame synthesis of catalysts.* Advanced Powder Technology, 2006. **17**(5): p. 457-480.
46. Madler, L., et al., *Direct formation of highly porous gas-sensing films by in situ thermophoretic deposition of flame-made Pt/SnO2 nanoparticles.* Sensors and Actuators B-Chemical, 2006. **114**(1): p. 283-295.